**Proceedings of the ASME 2010 3rd Joint US-European Fluids Engineering Summer Meeting and 8th International Conference on Nanochannels, Microchannels, and Minichannels**
**FEDSM-ICNMM2010**
**August 1-5, 2010, Montreal, Canada**

**FEDSM-ICNMM2010-30423**

# NUMERICAL INVESTIGATION OF LAMINAR FLOW AND HEAT TRANSFER IN MICRO-CYLINDER-GROUPS

**Ning Guan**
Energy Research Institute of Shandong Academy of Sciences
Jinan, Shandong, China

**Zhigang Liu**
Energy Research Institute of Shandong Academy of Sciences
Jinan, Shandong, China

**Masahiro Takei**
Department of Mechanical Engineering of Nihon University
Tokyo, Japan

**Chengwu Zhang**
Energy Research Institute of Shandong Academy of Sciences
Jinan, Shandong, China

## ABSTRACT

A numerical study on flow and heat transfer of de-ionized water over in-line and staggered micro-cylinder-groups had been performed with Reynolds number varying in the range from 0 to 150. A 3-D incompressible numerical model was employed to investigate the vortex distributions and the influences of the vortexes on the flow and heat transfer characteristics at low *Re* numbers in micro-cylinder-groups with different geometrical parameters, including micro-cylinder diameters (100μm, 250μm and 500μm), ratios of pitch to micro-cylinder diameter (1.5 2 and 2.5) and ratios of micro-cylinder height to diameter (0.5, 1, 1.5 and 2), etc. The vortex distributions, the flow and temperature fields, and the relationships among them were investigated by solving the numerical model with the finite volume method. It was found that the vortex number became larger with the increase of pitch ratio, and the change of flow rate distribution affected the heat transfer characteristics apparently. The appearance of vortexes in micro-cylinder-group increased the differential pressure resistance; as a result the total flow resistance in micro-cylinder-groups correspondingly increased. Meanwhile, the local heat transfer coefficients nearby the locations of vortexes greatly increased due to the boundary layer separation, which further enhanced the heat transfer in micro-cylinder-groups. The new correlations which could predict Nusselt number of de-ionized water over micro-cylinders with *Re* number varying from 0-150 had been proposed considering the differential pressure resistance and the natural convection based on numerical calculations in this paper.

## NOMENCLATURE

| | | |
|---|---|---|
| $a$ | Constant | |
| $b$ | Constant | |
| $D$ | Micro-cylinder diameter | m |
| $f$ | Friction factor | |
| $H$ | Micro-cylinder height | m |
| $L$ | Length of micro-cylinder-groups | m |
| $N$ | Micro-cylinder column number | |
| $p$ | Pressure | Pa |
| $\Delta p$ | Pressure difference between inlet and outlet | Pa |
| $q$ | Heat flux | |
| $S$ | Micro-cylinder-pitch ratio | m |
| $S_w$ | distance between the first row and the wall | m |
| $u$ | Velocity of x-direction | m/s |
| $u_{in}$ | x velocity at inlet | m/s |
| $v$ | Velocity of y-direction | m/s |
| $w$ | Velocity of z-direction | m/s |
| $x$ | x-coordinate | |
| $y$ | y-coordinate | |

 

| | | |
|---|---|---|
| $z$ | z-coordinate | |
| $\rho$ | Density of liquid water | $kg/m^3$ |
| $\mu$ | Viscosity of liquidwater | $m^2/s$ |
| 下标 | | |
| *in* | Inlet | |
| *outlet* | Outlet | |
| *symmetry* | Symmetry surface | |
| *wall_a* | Adiabatic walls | |
| *wall_h* | Heating walls | |
| *max* | Maximum | |

## INTRODUCTION

Driven by the rapid development of complementary metal oxide semiconductor, there are more and more investigations focusing on the enhanced micro-scale heat exchanger and the heat transfer mechanisms in these high efficiency structures in recent years. Micro-cylinder-groups can be used to enhance the convective heat transfer considering the perturbation of the micro-cylinders which may advance the flow transition from laminar to turbulent flow. However, the existence of the micro-cylinders may result in more complicated flow and heat transfer in micro-cylinder-groups.

Zhang et al. [1] experimentally investigated the friction factor characteristics of de-ionized water flow for both in-line and staggered arranged micro-cylinder-groups when the *Re* number varied in the range of 0 to 800. The friction factors in in-line and staggered micro-cylinder-groups with different micro-cylinder heights were obtained, which could be used to validate the numerical methods for the single flow of the micro-cylinder-groups.

Besides, some researchers carried out investigations on the flow and heat transfer of micro-pin-fins, which were also important references to explore the flow mechanism in micro-cylinder-groups. Mizunuma et al. [2] experimentally and numerically studied forced convective heat transfer from a micro-finned surface. It was found that the increased flow velocity in the free flow area above the fins in higher height channels yielded high heat transfer coefficients. Marques and Kelly [3] investigated heat transfer and pressure drop results for flat parallel plate and curved pin fin micro heat exchangers with a staggered arrangement with application to gas turbine blade cooling. It was concluded that the micro pin fin heat exchanger performance was better than a parallel plate counterpart, and the $k$–$\varepsilon$ turbulence model was the most commonly used model for prediction of thermal and hydrodynamic characteristics of pin–fin micro- heat exchangers. Lind [4] employed finite element method and several turbulence models to predict heat transfer and temperature distributions of pin fin micro-heat exchangers. The models included the standard $k$–$\varepsilon$ model (SKE), the renormalized group model (RNG), and the new $k$–$\varepsilon$ model.Galvis et al. [5] investigated the numerical models of pin-fin micro heat exchangers by employing several turbulence models using a 3D finite element model of a MHE. It was found that the flat micro pin fin heat exchanger overall thermal performance always exceeded that of the parallel plate counterpart (smooth channel) by a factor of as many as 2.2 for the 8.5mm diameter pins, and 4 for the 0.5 mm diameter pins in the investigated Reynolds number range. Further, the RNG model tended to be the best model to predict both the Nusselt number and the friction factor and capture the main feature of the flow field in MHE. Koşar et al. [6] carried out an experimental investigation on the pressure drops and friction factors associated with the forced flow of de-ionized water over staggered and in-line circular/diamond shaped micro pin-fin bundles 100 μm long with hydraulic diameter of 50 and 100 μm over *Re* number ranging from 5 to 128. Pin fins were arranged according to two different horizontal and vertical pitch ratios (1.5 and 5). This research found that the available large-scale correlations did not adequately predict the pressure drop at the micro scale. A modified correlation based on the experimental results obtained using micro scale devices had been proposed. The refined correlation accounted for in density and the endwall effects encountered in micro scale configurations. In addition, Koşar and Peles [7] also experimentally investigated the heat transfer and pressure drop of de-ionized water over a bank of shrouded staggered micro pin fins 243μm long with hydraulic diameter of 99.5 μm. Average heat transfer coefficients had been obtained for effective heat fluxes ranging from 3.8 to 167W/cm$^2$ and *Re* numbers from 14 to 112. It was found that for *Re* below 50 long tube correlations overpredicted the experimental *Nu* number, while at higher *Re* numbers existing correlations predicted the results moderately well. Endwall effect, which diminishes at high *Re* numbers, and a delay in flow separation for compact pin fins were attributed to the obtained trend. Peles et al. [8] investigated heat transfer and pressure drop over a bank of micro pin fins. A simplified expression for the total resistance was derived, discussed and experimentally validated. Geometrical and thermo-hydraulic parameters affecting the total thermal resistance were discussed. It was found that very low thermal resistances were achievable using a pin fin heat sink. The thermal resistance values were comparable with the data obtained in microchannel convective flows. In many cases, the increase in the flow temperature resulted in a convection thermal resistance, which was considerably smaller than the total thermal resistance. Naphon et al. [9] experimentally and numerically investigated the heat transfer characteristics of in-line and staggered taper pin fin heat sink under constant heat flux conditions. Experiments were performed at various *Re* numbers in the range of 1000-9000 and heat fluxes in the range of 0.91-3.64kW/m$^2$. The number of pin fins for in-line and staggered configurations were 16 and 17, respectively. The $k$-$\varepsilon$ standard turbulence model was employed to simulate the turbulent heat transfer characteristics. Compared with the experimental results, the numerical predictions were in reasonable agreement with the experiments. OHADI et al. [10] overviewed several thermal management techniques that could serve as an effective means to cool the next generation high flux electronics. These included the immersion cooling, jet impingement and spray cooling, and ultra thin film evaporation (UTF), particularly to serve at the chip level for hot spot cooling of the chip. The potential of these techniques for thermal management of current high flux electronics as well as the promise they hold for spot cooling of the next generation high flux electronics for commercial and military sectors were also discussed. Diez et al. [11] calculated the performance of micro-pin fins of variable diameter and rough surface by means of an approximate procedure based on truncated power series. Influence of surface roughness was evaluated for a wide range of heat transfer conditions; the results were discussed in terms of the two primary quantities of interest in fin design, viz., efficiency and effectiveness; then it could be safely applied to other geometric arrangements involving straight and annular fins due to the easiness of the present methodology.

Reviewing the literatures it can be known that the investigations on the single phase flow all focused on the pressure drops and the frictions factor characteristics, but detailed flow and temperature fields in micro-cylinder-groups, especially the vortex and temperature distributions in micro-cylinder-groups had not been investigated. Therefore, the present research numerically simulated laminar flow and heat transfer characteristics in the micro-cylinder groups and investigated the velocity field, the streamline distributions and the temperature field. Besides, the effects of the configurations of the micro-cylinder-groups on the flow field, the vortex distributions, and the heat transfer characteristics were also systematically analyzed.

## NUMERICAL MODELS

The physical geometry of the model for the micro-cylinder-group is schematically shown in Fig.1.

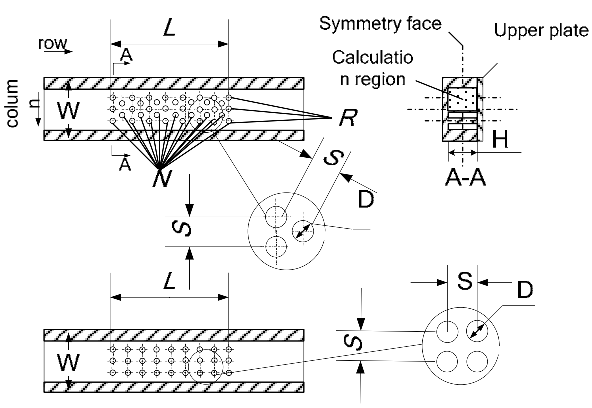


Fig. 1 Schematics of micro-cylinder-groups

The flow and heat transfer characteristics of seventeen micro-cylinder-group chips with different axial pitches *S*, the micro-cylinder heights *H*, the micro-cylinder diameters *D* and columns *N*, were numerically calculated in this paper. The widths *W* of all of the chips are 3.5mm and the detailed dimensions of the micro-cylinder-groups are listed in Table 1.

Table 1 Detailed dimension of the calculated chips of micro-cylinder-groups

| NO | *S*/*D* | *D*/μm | *H*/ μm | *L*/mm | *N* | arrangement |
|---|---|---|---|---|---|---|
| 1 | 1.5 | 500 | 250 | 14 | 5 | in-line |
| 2 | 2 | 500 | 250 | 14 | 5 | in-line |
| 3 | 2.5 | 500 | 250 | 15 | 5 | in-line |
| 4 | 2.5 | 500 | 500 | 15 | 5 | in-line |
| 5 | 2.5 | 500 | 750 | 15 | 5 | in-line |
| 6 | 2.5 | 500 | 1000 | 15 | 5 | in-line |
| 7 | 2 | 100 | 50 | 2.9 | 5 | in-line |
| 8 | 2 | 250 | 125 | 7.5 | 5 | in-line |
| 9 | 1.5 | 500 | 250 | 12.6 | 5 | staggered |
| 10 | 2 | 500 | 250 | 13.5 | 5 | staggered |
| 11 | 2.5 | 500 | 250 | 14.3 | 5 | staggered |
| 12 | 2 | 500 | 500 | 13.5 | 5 | staggered |
| 13 | 2 | 500 | 750 | 13.5 | 5 | staggered |
| 14 | 2 | 500 | 1000 | 13.5 | 5 | staggered |
| 15 | 2 | 500 | 250 | 16.9 | 10 | staggered |
| 16 | 2 | 500 | 250 | 20.4 | 15 | staggered |
| 17 | 2 | 500 | 250 | 23.8 | 20 | staggered |

Considering the structural symmetry of the micro-cylinder-group, a 3-D grid was generated based on 1/2 of the physical model (as shown in the left view of Fig.1) in the calculation, as shown in Fig.2. The girds of other chips were separately generated for the 17 micro-cylinder-groups listed in Tab.1.

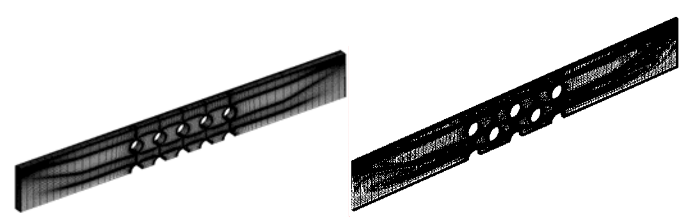

Fig.2 Grid generated for in-line and staggered micro-cylinder-groups

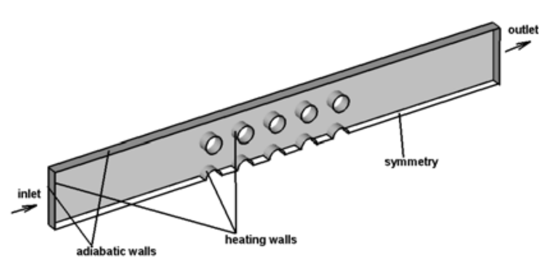


Fig.3 Boundary conditions for numerical models

In order to check the independency of the grid, the friction factor and *Nu* number was calculated based on four different girds with cells of 144000, 186000 and 255000, respectively. The deviation of friction factors among the three different grids was less than 5.1%, and the deviation of $Nu$ number was less than 7.4%. Therefore, the grid with 144000 cells achieved independent solution and was used to simulate the flow and heat transfer characteristics in present investigation.

In micro-scale flowing models, the Knudsen number is the criterion to judge whether the continuum model or rarefied flow model should be used. In this study the $Kn$ was found to be much less than $10^{-2}$, so that the continuum model could be used without any significant error to predict the flow field and the heat transfer characteristics of micro-cylinder-groups presented in Table 1. The 3-D laminar incompressible model was used to simulate the flow field when the liquid water flowed through the micro-cylinder-groups with $Re$ ranging from 0 to 150. Considering the natural convection in micro-cylinder-groups at high heat flux may affect the heat transfer characteristics, the Boussinesq assumption was employed to simulate the significance of mixed convection in present investigation. The governing equations of the model are:

$$\mathrm{Re}=\frac{\rho u_{\max} D}{\mu} \tag{1}$$

$$\frac{\partial u}{\partial x}+\frac{\partial v}{\partial y}+\frac{\partial w}{\partial z}=0 \tag{2}$$

$$\frac{\partial \rho uu}{\partial x}+\frac{\partial \rho uv}{\partial y}+\frac{\partial \rho uw}{\partial z}=-\frac{\partial p}{\partial x}+\frac{\partial}{\partial x}(\mu\frac{\partial u}{\partial x})+\frac{\partial}{\partial y}(\mu\frac{\partial u}{\partial y})+\frac{\partial}{\partial z}(\mu\frac{\partial u}{\partial z}) \tag{3}$$

$$\frac{\partial \rho vu}{\partial x}+\frac{\partial \rho vv}{\partial y}+\frac{\partial \rho vw}{\partial z}=-\frac{\partial p}{\partial y}+\frac{\partial}{\partial x}(\mu\frac{\partial u}{\partial x})+\frac{\partial}{\partial y}(\mu\frac{\partial u}{\partial y})+\frac{\partial}{\partial z}(\mu\frac{\partial u}{\partial z}) +\rho g\beta(T-T_c) \tag{4}$$

$$\frac{\partial \rho wu}{\partial x}+\frac{\partial \rho wv}{\partial y}+\frac{\partial \rho ww}{\partial z}=-\frac{\partial p}{\partial z}+\frac{\partial}{\partial x}(\mu\frac{\partial w}{\partial x})+\frac{\partial}{\partial y}(\mu\frac{\partial w}{\partial y})+\frac{\partial}{\partial z}(\mu\frac{\partial w}{\partial z}) \tag{5}$$

$$\frac{\partial \rho uT}{\partial x}+\frac{\partial \rho vT}{\partial y}+\frac{\partial \rho wT}{\partial z}=\frac{\partial}{\partial x}(\frac{\lambda}{C_p}\frac{\partial T}{\partial x})+\frac{\partial}{\partial y}(\frac{\lambda}{C_p}\frac{\partial T}{\partial y})+\frac{\partial}{\partial z}(\frac{\lambda}{C_p}\frac{\partial T}{\partial z}) \tag{6}$$

The parameter $u_{max}$ is the average velocity on the minimum flow cross section along flowing direction, which can be calculated by the following equation:

$$u_{\max}=u_{in}\frac{S}{S-D} \tag{7}$$

The boundary conditions (as shown in Fig.3) for the numerical model consisting of walls (including heating walls and adiabatic walls), a velocity inlet, a full developed outlet and two symmetry planes are expressed as follows:

$$u,v,w\,|_{wall\_h}=0,\quad \left.\frac{\partial T}{\partial \vec{n}}\right|_{wall\_h}=q,\quad u,v,w\,|_{wall\_a}=0,$$

$$\left.\frac{\partial T}{\partial \vec{n}}\right|_{wall\_h}=0,\quad u\,|_{inlet}=U_{in},\quad v,w\,|_{inlet}=0,\quad T\,|_{inlet}=293.15K,$$

$$\left.\frac{\partial u}{\partial \vec{n}}\right|_{outlet}=0,\quad \left.\frac{\partial v}{\partial \vec{n}}\right|_{outlet}=0,\quad \left.\frac{\partial w}{\partial \vec{n}}\right|_{outlet}=0,\quad \left.\frac{\partial T}{\partial \vec{n}}\right|_{outlet}=0,$$

$$\left.\frac{\partial u}{\partial \vec{n}}\right|_{symmetry}=0,\quad v\,|_{symmetry}=0,\quad \left.\frac{\partial w}{\partial \vec{n}}\right|_{symmetry}=0,$$

$$\left.\frac{\partial T}{\partial \vec{n}}\right|_{symmetry}=0$$

The finite volume method was used to obtain the discrete models of the governing equations which can be solved by SIMPLE algorithm. The equations (1)-(6) are solved by C++ language program.

The 3-D velocity fields and temperature fields in micro-cylinder-groups listed in Table 1 can be predicted by the numerical methods above and then the friction factor $f$ and $Nu$ number of the laminar flow in the micro-cylinder-group can be calculated by:

$$f=\frac{2\Delta pD}{\rho u_{\max}^2 L},\ Nu=hD/\lambda \tag{8}$$

## RESULTS AND DISCUSSIONS

Figure 4 shows the velocity fields and enlarged velocity distributions on the symmetry faces along the x-direction (which is also the flowing direction) in in-line arrayed micro-cylinder-groups with different pitches of $S/D$=1.5, 2, 2.5, respectively.

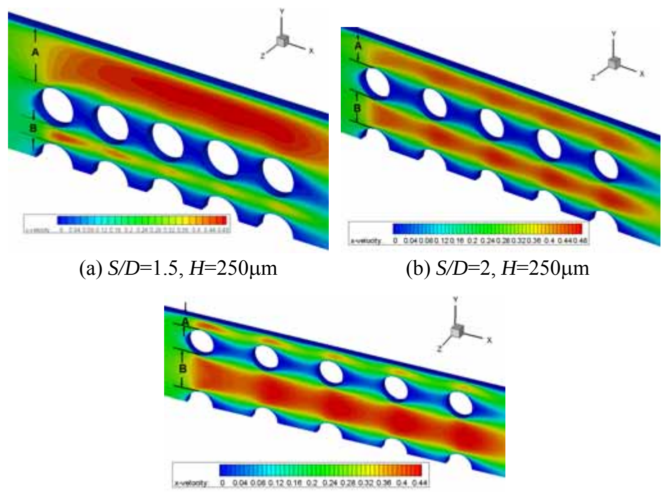

(a) $S/D$=1.5, $H$=250μm (b) $S/D$=2, $H$=250μm

(c) $S/D$=2.5, $H$=250μm

Fig.4 Velocity fields of the micro-cylinder-groups with different pitches (in-line array arrangement) at $Re$=75

In Fig.4 (a), five high-speed narrow regions appear in area B between the two micro-cylinders of each column. The area of the high-speed region corresponding to the first four columns is reduced and the value of the highest speed in this region decreases along the flowing direction. However, the area of high-speed region between the two micro-cylinders of the fifth column is larger than that of the fourth column, and the highest speed increases simultaneously. Different from the micro-cylinder-groups with $S/D$=1.5, the high-speed regions for the chip NO.2 of $S/D$=2 in area B are so large that they link with each other and form a interchange region which is almost parallel with the high-speed region in area A, as shown in Fig.4(b). Besides, the total area of the high-speed region in area A is almost equal with that of area B, because the width of area B is almost the same as that of area A. Increasing the pitch to $S/D$=2.5, as illustrated in Fig. 4(c), the velocity distributions in areas A and B are opposite to those of $S/D$=1.5. Five high-speed narrow regions appear in area A near the wall. Similar to $S/D$=1.5, the area of the high-speed region and the value of the highest speed in the region are both reduced along the flowing direction until the location of the fourth micro-cylinder, but the fifth high-speed region is almost the same as the fourth one.

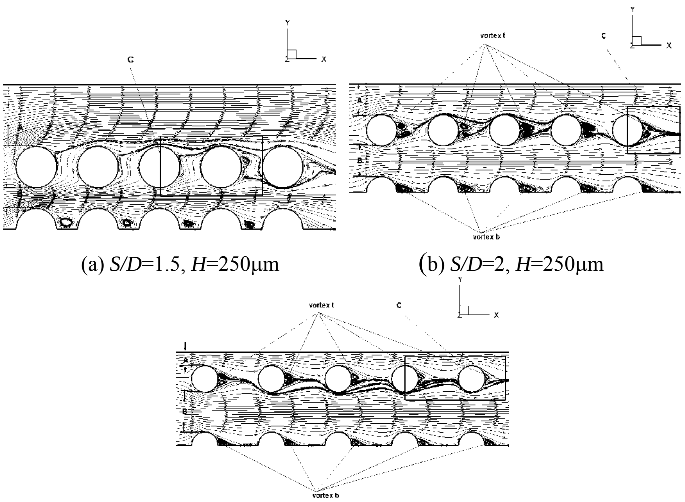


(a) $S/D$=1.5, $H$=250μm (b) $S/D$=2, $H$=250μm

(c) $S/D$=2.5, $H$=250μm

Fig.5 Streamline distributions on the symmetry face with different pitches (in-line array arrangement) at $Re$=75

Figure 5 shows the comparisons of the streamline distributions in in-line arranged micro-cylinder-groups with different pitches. In Fig. 5(a), there is no vortex along the flowing direction behind the first and the second micro-cylinder in the row close to the wall due to strong interaction among micro-cylinders at $S/D$=1.5, although a part of fluid flows into area A behind the first two columns micro-cylinders. As the increase of the flow resistance, a counter-clockwise vortex whose center is below the axis of the micro-cylinder appears in the leeside of the third micro-cylinder in the row close to the wall and there is still some fluid flowing into area A from area B. Then a clockwise vortex appears behind the fourth micro-cylinder due to the increase of the viscous resistance loss, so some fluid begins to flow into area B from area A. Increasing the micro-cylinder pitch to $S/D$=2, the interactions among the micro-cylinders decrease apparently compared with $S/D$=1.5. As a result, a couple of vortexes appear behind each micro-cylinder in the row close to the wall, as shown in Fig. 5(b). For the first three vortex couples, the clockwise vortex $t$ is a little nearer to the micro-cylinder and it is smaller than vortex $b$, so some fluid flows into area B from area A through the leesides of these three micro-cylinders. However, the location of clockwise vortex becomes further from the micro-cylinder, and its area is a little larger than the counter-clockwise one when the fluid flows by the fourth micro-cylinder, so some fluid flows into area B from area A across the leeside of this fourth micro-cylinder, as shown in Fig. 5(b). Keep increasing the pitch to $S/D$=2.5, the total number of vortexes appearing in the micro-cylinder-group is equal to that in the one of $S/D$=2, but the vortexes behind the micro-cylinders become small and the evolution law of the vortexes along the flowing direction is opposite to that of $S/D$=2. In Fig. 5(c), the clockwise vortex behind each micro-cylinder in the row close to the wall is larger at first and then is smaller than the counter-clockwise one along the flowing direction, so the flow rate distribution of the fluid in area A and B is opposite to the micro-cylinder-group with $S/D$=2.

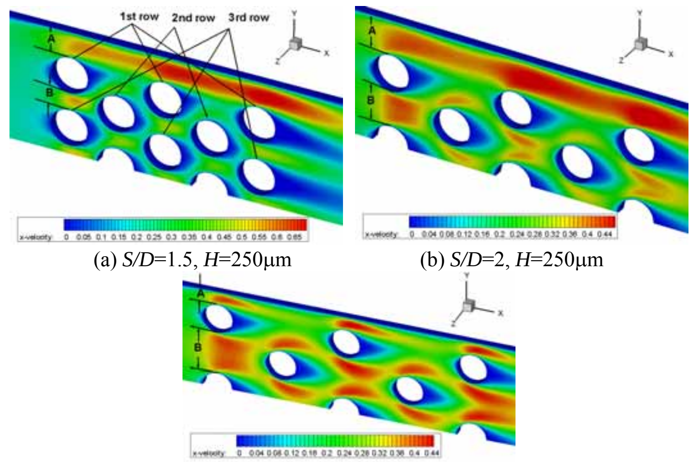


(a) $S/D$=1.5, $H$=250μm (b) $S/D$=2, $H$=250μm

(c) $S/D$=2.5, $H$=250μm

Fig.6 Velocity fields of micro-cylinder-groups with different pitches (staggered array arrangement) at $Re$=75

The three-dimensional velocity field of the liquid water flowing through the staggered micro-cylinder-groups with different pitches of $S/D$=1.5, 2, 2.5, respectively, are illustrated in Fig.6. It can be known that there are apparent differences about the velocity distribution between in-line and staggered micro-cylinder-groups. For in-line array arrangement, the velocity in the leeside region of each micro-cylinder is low and several high-speed regions induced by the fluid viscosity appear between the micro-cylinders in each column. However, a high-speed area like a butterfly appears in the leeside region of each micro-cylinder for staggered array arrangement due to the superposition of the velocity fields around the neighbor micro-cylinders, as shown in Fig. 6. The shapes and the edges of the high-speed regions like butterfly in the micro-cylinder-group with smaller pitch of $S/D$=1.5 are not as clear as those of $S/D$=2 and 2.5, as shown in Fig. 6(a), (b) and (c), In addition, the areas of low-speed region behind each micro-cylinder with the pitch of $S/D$=1.5 are smaller than those of $S/D$=2 and 2.5 due to the strong interaction among the micro-cylinders.

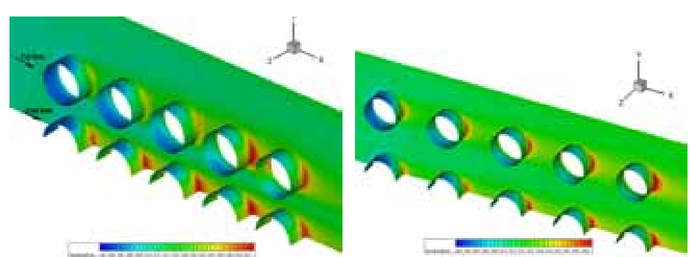

 

(a) $S/D$=1.5, $H$=250μm (b) $S/D$=2, $H$=250μm

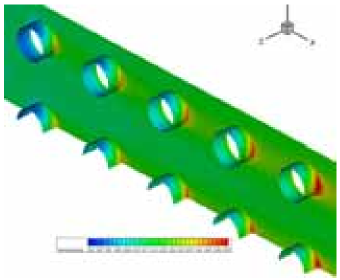

(c) $S/D$=2.5, $H$=250μm

Fig.7 Temperature fields of the micro-cylinder-groups with different pitches (in-line array arrangement) at $Re$=75

Temperature distributions at $q$=15W/cm$^2$, $Re$=75 for in-line arranged micro-cylinder-groups with pitch ratios of 1.5, 2, 2.5 are shown in Fig.7. It can be known that the temperatures in upwind ward of the micro-cylinder are low, which is attributed to the enhancement of heat transfer at high flowing velocities. However, the heat transfer coefficient becomes smaller for the lower flow velocity when the liquid flows into the lee ward of the micro-cylinder, and thus a high temperature region appears in the lee ward of each micro-cylinder. As it is known that the boundary layer along the micro-cylinder surface separates from the lee side due to the liquid viscosity, consequently the local heat transfer coefficient increases apparently at this point, so the temperatures is low in the region near the separating point, as shown in Figs. 7. Besides, it also can be seen from the comparisons among (a), (b) and (c) of Fig.7.that the area of the high temperature region in the lee ward of micro-cylinder with $S/D$=1.5 increases along the flowing direction until the fourth column, and then it begins to decrease, especially for the 1$^{st}$ row of micro-cylinders. As seen in Fig.4, we know that the velocity distribution of incoming flow for each micro-cylinder varies during the flow and the velocity at the same location near the wall in the lee ward of the micro-cylinder decreases a little along the flowing direction according to the simulation results, although the total flow rate keeps a constant. Therefore, the heat transfer in the lee wards of downstream micro-cylinders is weaker than that of the upstream ones and the area of high temperature region in the lee ward of micro-cylinder increases along the flowing direction. Furthermore, a large vortex (as shown in Fig. 5(a)) appears in the lee ward of the fourth micro-cylinder due to the effect of the viscous force and flow velocities in this vortex region become lower, so the local heat transfer coefficient drops and the temperatures rises. However, the average velocity in the lee ward of the fifth micro-cylinder a little increases with the sudden disappearance of the vortex, at the same time the area of the high temperature region decreases slightly compared with that of the fourth micro-cylinder. For the 2$^{nd}$ row of micro-cylinders on the symmetry surface, the liquid flow rate distribution in different regions changes along the flowing direction due to the influence of the 1$^{st}$ row micro-cylinders, as shown in Fig.5 (a). A part of fluid flows from region B to region A through the lee wards of the first three columns, thus the flow rate and average velocity of the lee ward of each micro-cylinder decreases, so does the local heat transfer coefficient. However, the flow rate distribution changes again with the appearance of the vortex in the lee ward of the fourth column micro-cylinder in the 1$^{st}$ row when the liquid flows by the fourth column micro-cylinder, and a part of fluid flows from region A to region B through the lee ward of the fourth micro-cylinder of the 1$^{st}$ row, as shown in Fig. 5(a). As a result, the average velocity and the local heat transfer coefficient in the lee ward of the fifth micro-cylinder in the 2$^{nd}$ row increase, correspondingly, the area of the high temperature region decreases. Increasing the pitch of micro-cylinders to $S/D$=2, 2.5, the flow rate distribution changes not as apparently as that of the micro-cylinder-groups with $S/D$=1.5 because one couple vortexes appear behind each micro-cylinder, so the area of the high temperature region in the lee ward of each micro-cylinder decreases along the flowing direction. Besides, the average surface temperature of micro-cylinder for $S/D$=1.5 is a little lower than that of $S/D$=2, 2.5 due to the heat transfer enhancement as a result of strong changes of flow rate distribution in the micro-cylinder-group with smaller pitch ratios, which can be known from the comparison among Fig.7(a), (b) and (c). In addition, the temperature difference between the bottom and the top of the micro-cylinder is higher in micro-cylinder-groups with $S/D$=1.5, 2 than that of $S/D$=2.5, so the natural convective heat transfer becomes stronger and the total heat transfer in micro-cylinder-groups is enhanced.

Figure 8 shows the temperature distributions at $q$=15W/cm$^2$, $Re$=75 in staggered arranged micro-cylinder-groups with pitches of 1.5, 2, 2.5, respectively. It can be known by comparing Fig.8 with Fig.7 that the temperature distribution on the wall varies very little with the change of pitch ratio in staggered micro-cylinder-groups compared with that in in-line arrangement, and the area of high temperature region continuously increases along the flowing direction. For the staggered micro-cylinder-groups with $S/D$=1.5, the area of the high temperature region in lee ward of the micro-cylinder is smaller than that in micro-cylinder-groups of $S/D$=2, 2.5, which resulted from the stronger interactions among the micro-cylinders at lower $S/D$. Besides, the average temperature difference between the upwind side and lee side of micro-cylinders in micro-cylinder-group of $S/D$=1.5 is lower than that of $S/D$=2, 2.5, as shown in Fig. 8(a), (b) and (c), therefore the lower pitch ratio can enhance the heat transfer in micro-cylinder-groups.

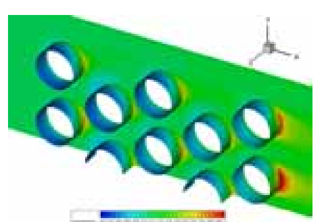

(a) $S/D$=1.5, $H$=250μm

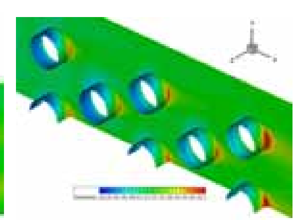

(b) $S/D$=2, $H$=250μm

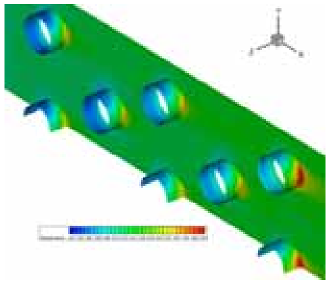

(c) *S/D*=2.5, *H*=250μm

Fig.8 Temperature fields of the micro-cylinder-groups with different pitches (staggered array arrangement) at *Re*=75

Profiles of heat transfer coefficients vs. *Re* in in-line and staggered arranged micro-cylinder-groups with different pitch ratios and micro-cylinder heights are illustrated in Figs.9-10 and Figs.11-12, respectively.

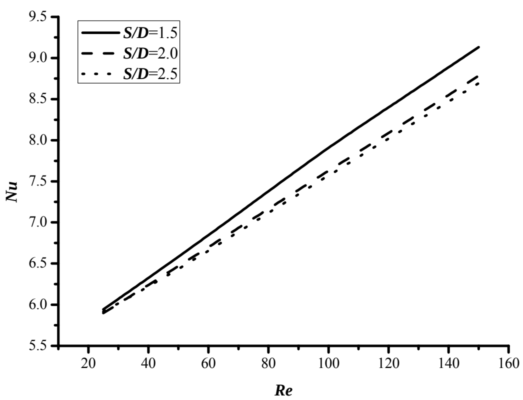


Fig.9 *Nu* numbers in micro-cylinder-groups with different pitches(in-line array arrangement)

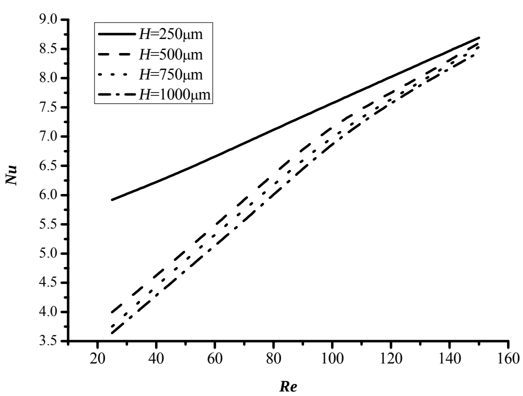


Fig.10 *Nu* numbers in micro-cylinder groups different heights of cylinders (in-line array arrangement)

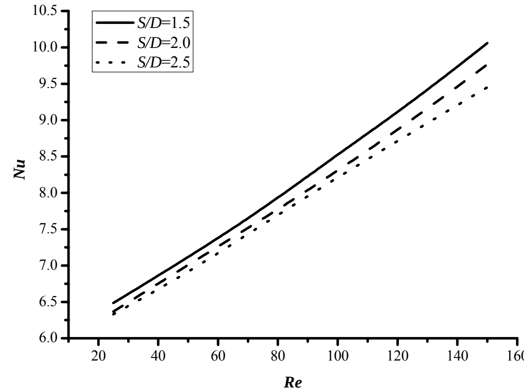


Fig.11 *Nu* numbers in micro-cylinder-groups with different pitches(staggered array arrangement)

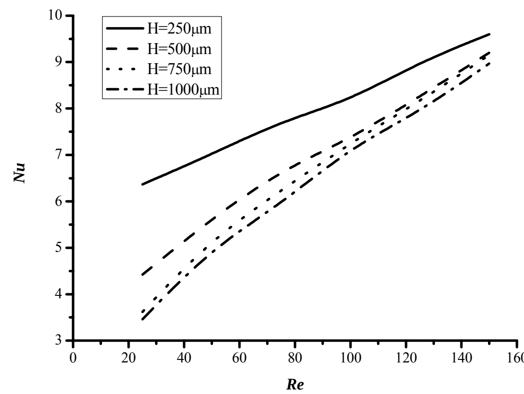


Fig.12 Nu nmubers in micro-cylinder groups with different heights of cylinders(staggered array arrangement)

It can be known from comparisons that the *Nu* number increases with the decrease of the pitch ratio for both in-line and staggered micro-cylinder-groups. This phenomenon is caused by the stronger change of flow rate distribution and the fluid mixture among different regions in micro-cylinder-groups with *S/D*=1.5, as a result the heat transfer is enhanced. Comparing the micro-cylinder-groups with different cylinder heights, it is known that the *Nu* number increases with the decrease of micro-cylinder height at low *Re* numbers, especially when the micro-cylinder-groups height is larger than the micro-cylinder diameter, as shown in Fig.10 and Fig.12. As discussed by Sparrow[12], the wall boundary layer thickness extends a few micro-cylinder diameters from the wall at lower *Re* number, which can strongly affect the hydrodynamic field (end-wall effect), so the total flow channel is immersed in the fluid for the micro-cylinder-groups investigated in present paper (0.5≤*H/D*≤2). Thus, the velocity gradients near the wall in micro-cylinder-groups rapidly increase with the decrease of micro-cylinder height, so the fluid velocity at the location with same distance from the wall is higher in micro-cylinder-groups with larger height and the heat transfer is enhanced. However, the *Nu* number discrepancies in micro-cylinder-groups for different micro-cylinder heights become smaller with increase of *Re* number, which is attributed to the weakness of end-wall effect, especially for the micro-cylinder-groups with large micro-cylinder height.

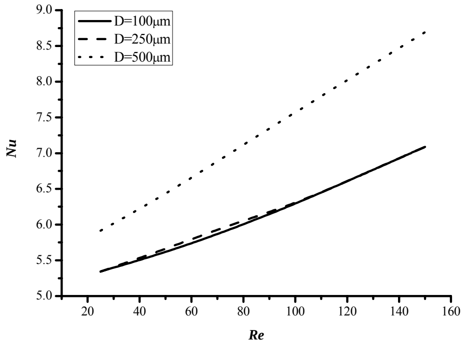


Fig.13 *Nu* numbers of micro-cylinder-groups with different diameters

Comparisons of *Nu* numbers in micro-cylinder-groups with different cylinder diameters are illustrated in Fig.13. It can be known from Fig. 13 that *Nu* numbers become larger with the increase of micro-cylinder diameter. This may be attributed to the drastic change of thermal properties of the working fluid in micro-cylinder-groups with small cylinder diameters. It is known that the temperature of water increases rapidly along flow direction at low *Re* numbers in micro-cylinder-groups with smaller cylinder diameters, as a result, the Prandtl number of water decreases more apparently than that in micro-cylinder-groups with larger cylinder diameters under the same heat flux, therefore the *Nu* number becomes smaller with the decrease of cylinder diameter, as shown in Fig.13.

The flow and heat transfer characteristics in micro-cylinder-groups can be evaluated by friction factor *f* and *Nu*, respectively. The friction factor in micro-cylinder-groups is decided by $\rho$, $u_{max}$, $\mu$, $H$, $S$, $D$, $L$, $S_w$, and *Nu* is decided by the parameters of $\rho$, $u_{in}$, $\mu$, $Cp$, $\lambda$, $H$, $S$, $D$, $L$. According to Rayleigh dimensional method, the friction factor *f* and *Nu* number of the liquid flow in micro-cylinder-groups can be described by:

$$f = k\rho^{a1} u_{\max}^{a2} \mu^{a3} H^{a4} S^{a5} D^{a6} L^{a7} S_w^{a8} \tag{9}$$

$$Nu = k\rho^{b1} u_{\max}^{b2} \mu^{b3} C_P^{b4} \lambda^{b5} S^{b6} D^{b7} L^{b8} H^{b9} \tag{10}$$

According to the dimensional analysis, the following equation can be obtained from Eq. (9)-(10):

$$f = k(ML^{-3})^{a1} (Lt^{-1})^{a2} (ML^{-1}t^{-1})^{a3} L^{a4+a5+a6+a7+a8} \tag{11}$$

$$Nu = k(ML^{-3})^{b1} (Lt^{-1})^{b2} (ML^{-1}t^{-1})^{b3} (L^2 t^{-2} T^{-1})^{b4} (MLt^{-3} T^{-1})^{b5} L^{b6+b7+b8+b9} \tag{12}$$

The relationships of the powers in Eq. (9) and Eq.(10) are given by following equations respectively:

$$a_1 = a_2 = -a_3\,,\quad a_6 = -a_3 - a_4 - a_5 - a_7 - a_8 \tag{13}$$

$$b_1 = b_2\,,\quad b_4 = -b_5\,,\quad b_1 = b_6 + b_7 + b_8 + b_9 \tag{14}$$

Therefore, Eq. (9)-(10) can be re-written as:

$$f = k\frac{\rho^{-a_3} u_{\max}^{-a_3} D^{-a_3}}{\mu^{-a_3}} H^{a_4} S^{a_5} D^{a_6} L^{a_7} S_w^{a_8} \tag{15}$$

$$Nu = k\left(\frac{\rho u_{\max} D}{\mu}\right)^{b1} \left(\frac{C_p \mu}{\lambda}\right)^{b4} \frac{S^{b_6} L^{b_8} H^{b_9}}{D^{b_6+b_8+b_9}} \tag{16}$$

Basing on the numerical results for different cases, the powers in Eq. (11)-(12) can be obtained. Then the friction factor *f* and *Nu* number of the laminar liquid flow in the micro-cylinder-group with *Re* ranging from 0 to 150 can be predicted by the following correlation:

In-line array arrangement：

$$f = 0.26\,\mathrm{Re}^{-0.765}\left(\frac{H}{D}\right)^{-0.717}\left(\frac{S}{D}\right)^{0.0151}\left(\frac{L}{D}\right)^{1.192}\left(\frac{S_w}{D}\right)^{1.158}$$

For $0 \le Re \le 150$, $100\mu m \le D \le 500\mu m$, water (17)

$$Nu = 1.073\,\mathrm{Re}^{0.752}\,\mathrm{Pr}^{0.386}\left(\frac{S}{D}\right)^{-0.04}\left(\frac{L}{D}\right)^{-0.552}\left(\frac{H}{D}\right)^{-0.397}$$

For $0 \le Re \le 150$, $100\mu m \le D \le 500\mu m$, water (18)

Staggered array arrangement:

$$f = 0.079\,\mathrm{Re}^{-0.443}\left(\frac{H}{D}\right)^{-0.722}\left(\frac{S}{D}\right)^{-3.051}\left(\frac{L}{D}\right)^{1.904}\left(\frac{S_W}{D}\right)^{-1.469}$$

For $0 \le Re \le 150$, $100\mu m \le D \le 500\mu m$, water (19)

$$Nu = 1.059\,\mathrm{Re}^{0.807}\,\mathrm{Pr}^{0.279}\left(\frac{S}{D}\right)^{-0.059}\left(\frac{L}{D}\right)^{-0.356}\left(\frac{H}{D}\right)^{-0.273}$$

For $0 \le Re \le 150$, $100\mu m \le D \le 500\mu m$, water (20)

The predictions of correlation Eq. (19) are compared with experimental results [1] and prediction of Kosar's correlation [6], as shown in Fig.14.

Kosar Correlation is as follows:

$$f = \frac{7259}{\mathrm{Re}^{1.7}}\left(\frac{H/D}{H/D+1}\right)^{1.9}\left(\frac{S^2}{Ac}\right)^{-0.4} + \frac{54}{\mathrm{Re}_d^{0.7}}\left(\frac{1}{1+H/D}\right)^{2.0}\left(\frac{S^2}{Ac}\right)^{-0.7}$$

$$\mathrm{Re}_d = \frac{\rho u_{\max} d_h}{\mu}\,,\quad d_h = \frac{4A_{\min}L}{A}\,,\quad A = \pi DHN + 2\left(WL - \frac{\pi D^2}{4}N\right),$$

$$A_{\min} = RH(S-D) \tag{21}$$

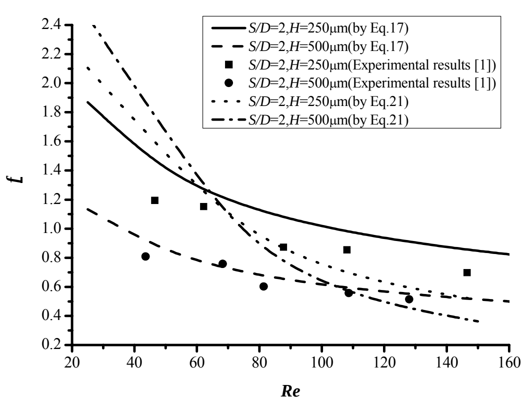


Fig. 14 Comparisons of friction factors for in-line arrangement between predictions and experimental results and Kosar's correlation

 

From the comparisons of the numerical and experimental friction factor in Fig.14, it is known that the deviations between the predictions of Eq. (21) and the experimental results are apparently larger than those of Eq. (19), especially for $Re \leq 100$. The predictions of Eq.(19) are higher than experimental results[1], and the maximum discrepancy is 22.3% for micro-cylinder-groups of $H$=250μm, and 13.2% for that of $H$=500μm. These discrepancies may be attributed to the tip clearance in the experimental investigations. Considering the ratio of the tip clearance to the height may be larger in micro-cylinder-groups of $H$=250μm than that of $H$=500μm, so the influence of tip clearance on flow characteristics becomes more obvious with decrease of micro-cylinder height. Moreover, the end-wall effect affects the flow in micro-cylinder-groups of $H$=250μm more apparently than that of $H$=500μm, so the decrease of flow resistance caused by tip clearance may be larger for micro-cylinder-groups with $H$=250μm, as shown in Fig.14.

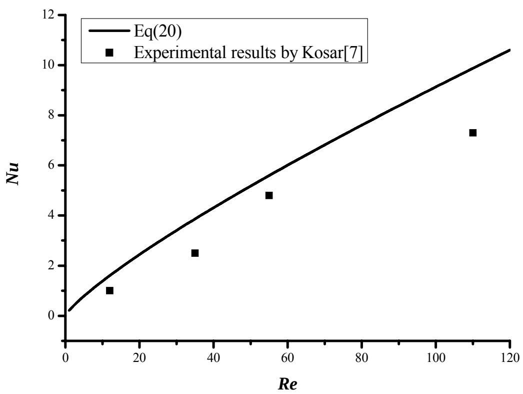


Fig. 15 Comparisons of heat transfer coefficients for staggered arrangement between predictions and experimental results [7]

Figure15 illustrates the comparisons between the correlation Eq. (20) and the experimental results [7]. It can be known that the predictions of correlation obtained in present investigation are higher than experimental results, and the maximum deviation is about 35.2% ($Re$=112). As mentioned above, two assumptions have been made in boundary conditions: the heat fluxes on bottom wall and micro-cylinder walls are constant (15W/cm$^2$); the top wall and side walls are adiabatic. But in experimental investigations, heating elements were deposited on the back side of the silicon chips, and experimental chips were heated by the heating element from the bottom side. Considering the thermal conductivity of silicon is relatively low, the heat flux on the micro-cylinder walls is lower than that on the bottom walls of micro-cylinder-groups in experiments. As a result, the experimental $Nu$ numbers are lower than the predictions of correlation. Besides, a part of fluid may flow through the tip clearance between the micro-cylinder tips and the top wall, and thus the effect of tip clearance further reduces the experimental results. Therefore, the predictions of correlation are higher than experimental results with comprehensive actions of these factors although there is heat loss that may influence the experimental $Nu$ numbers during the experimental process. In addition, the ratio of the flow rate flowing through the tip clearance to the total flow rate may be large with the increase of $Re$ number, and so the discrepancies of $Nu$ number between the predictions and experimental results become large with the increase of $Re$ number, as shown in Fig.15.

## 5. Conclusions

The flow and heat transfer characteristics of laminar state in staggered and in-line arranged micro-cylinder-groups were numerically investigated with $Re$ number varying from 0-150. The vortex distribution and temperature field of laminar flow were analyzed for micro-cylinder-groups with different pitch ratios, micro-cylinder heights, micro-cylinder diameters and column numbers. The concluding remarks are as follows in present paper:

(1) For in-line arrangement, the vortex number and area changes with the pitch ratio of micro-cylinder-groups attributed to in laminar flow field. The friction resistance and differential pressure resistance varies with the change of pitch ratio in micro-cylinder-groups, and the friction factors increases with the decrease of pitch ratio due to stronger interactions among the micro-cylinders;

(2) A high temperature region exists in the lee ward of every micro-cylinder for in-line and staggered micro-cylinder-groups, and the area of this region increases at first and then decreases along the flowing direction for the in-line arrangement with $S/D$=1.5. For staggered arrangement, the area of this high temperature region decreases along the flowing direction and it becomes larger with the increase of pitch ratio. As a result, the heat transfer in micro-cylinder-groups can be enhanced by decreasing the pitch ratio for both in-line and staggered arrangement;

(3) The structural parameters of the micro-cylinder group, such as pitch ratio, micro-cylinder height, column number and micro-cylinder diameter, etc., may all influence the heat transfer characteristics, among which the effects of micro-cylinder height and diameter on heat transfer coefficients are more significant than the other parameters. For $Re \leq 150$, the discrepancy of heat transfer coefficient in micro-cylinder-groups with different micro-cylinder height becomes smaller with the increase of $Re$ number, but it becomes larger for the micro-cylinder-groups with different diameter;

(4) New correlations of $f$ and $Nu$ accounting for the effect of structural parameters and the mixed convection had been developed for in-line and staggered micro-cylinder-groups (without considering the tip clearance effect), which can be used to predict the characteristics of laminar flow and heat transfer.

## ACKNOWLEDGMENTS

The authors acknowledge the support of Research grant of Japan Society of the Promotion Science (#21360088), Project Research of CST (Nihon University, Prof. Takei's lab) and National Science Foundation of China under Grant No. 50976062.

## REFERENCES

[1] Zhang C. W., Liu Z. G., Guan N., 2009, "Experimental Investigations on the Resistance Characteristics of Micro-Cylinder-Groups" , J. Eng. Thermophys., vol.30, pp.1898-1900.

[2] Mizunuma H., Behnia M., Nakayama W., 1997, "Heat Transfer from Micro-Finned Surfaces to Flow of Fluorinert Coolant in Reduced-Size Channels", IEEE Trans Components Packaging Manuf. Technol., Part A, vol.20(2):139–145.

[3] Marques C., Kelly K.W., 2004, "Fabrication and Performance of a Pin Fin Micro Heat Exchanger", ASME J. Heat Transfer vol.126:434–444.

[4] Lind E.K., 2002, "Analysis of Turbulence Models in a Cross Flow Pin Fin Micro-Heat Exchanger". M.Sc. Thesis, Naval Postgraduate School, Monterey.

[5] Gaivis E., Jubran B. Xi A., Behdinan F., K., 2008, "Numerical Modeling of Pin-Fin Micro Heat Exchangers", Heat Mass Transfer, vol.44, pp.659-666.

[6] Koşar A., Mishra C., Peles Y., 2005, "Laminar Flow Across a Bank of Low Aspect Ratio Micro Pin Fins", J. Fluids Eng., vol.127, pp.419-430.

[7] Koşar A., Peles Y., 2006, "Thermal-Hydraulic Performance of MEMS-Based Pin Fin Heat Sink", J. Heat Transfer, vol.128, pp.121-131.

[8] Peles Y., Koşar A., Chandan M., Kuo C. J., Schneider B., 2005, "Forced Convective Heat Transfer Across A Pin Fin Micro Heat Sink", Int. J. Heat Mass Transfer, vol.48, pp.3615-3627.

[9] Naphon P., Sookkasem A., 2007, "Investigation on Heat Transfer Characteristics of Tapered Cylinder Pin Fin Heat Sinks", Energy Convers. Manage., vol.48, pp.2671-2679.

[10] Ohadi M., Qi J., Lawler J., 2004, "Ultra-Thin Film Evaporation(UTF)-Application to Emerging Technologies in Cooling of Microelectronics", Microscale Heat Transfer, pp. 321-338.

[11] Diez L. I., Espatolero S., Cortes C., Campo A., 2009, "Thermal Analysis of Rough Micro-Fins of Variable Cross-Section by the Power Series Method", Int. J. Therm. Sci., ,online.

[12] Sparrow E. M., Kang S. S., 1985, "Longitudinally-Finned Cross Flow Tube Banks and Their Heat Transfer and Pressure Drop Characteristics", Int. J. Heat Mass Transfer, 28(2), pp.339-350.

 